THE JOURNAL OF PHYSICAL CHEMISTRY C

pubs.acs.org/JPCC Article

Unraveling Direct and Indirect Energy Transfer Pathways in a Light-Harvesting Dendrimer

Maria Camila Aguilera, Adrian E. Roitberg, Valeria D. Kleiman, Sebastian Fernandez-Alberti, and Johan F. Galindo*

Cite This: J. Phys. Chem. C 2020, 124, 22383−22391 Read Online

ACCESS | Metrics & More | Article Recommendations | Supporting Information

ABSTRACT: Light-harvesting and intramolecular energy funneling are fundamental processes in natural photosynthesis. A comprehensive knowledge of the main structural, dynamic, and optical properties that regulate the efficiency of such processes can be deciphered through the study of artificial light-harvesting antennas, capable of mimicking natural systems. Dendrimers are some of the most explored artificial light-harvesting molecules. However, they have to be well-defined and highly branched conjugated structures, creating intramolecular energy gradients that guarantee efficient and unidirectional energy transfer. Herein, we explore the contributions of the different mechanisms responsible for the highly efficient energy funneling in a large, complex poly(phenylene−ethynylene) dendrimer, whose architecture was particularly designed to conduct the initially absorbed photons toward a spatially localized energy sink away from its surface, avoiding its quenching by the environment. For this purpose, the nonradiative photoinduced energy relaxation and redistribution are simulated by using nonadiabatic excited state molecular dynamics. In this way, the two possible direct and indirect pathways for exciton migrations, previously reported by time-resolved spectroscopy, are defined. Our results stimulate future developments of new synthetic dendrimers for applications in molecular-based photonic devices in which an enhancement in the photoemission efficiency can be predicted by changes in the detailed balance between the different intramolecular energy transfer pathways.

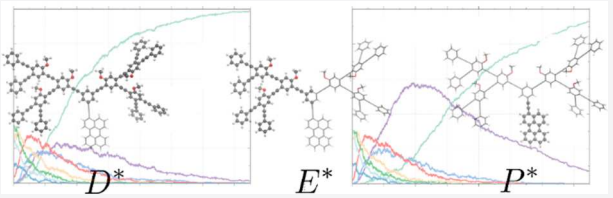

INTRODUCTION

Nature provides numerous examples of how organisms have evolved the ability to convert light into chemical energy through the use of conjugated chromophores that efficiently funnel the absorbed energy to a reaction center.[1−6] In the wake of the study of natural systems, researchers have focused their efforts on the design and synthesis of new light-harvesting materials for improved power conversion efficiency of organic photovoltaic devices.[2,7−11]

Light-harvesting dendrimers are conjugated and highly branched macromolecules, composed of well-defined arrays of weakly coupled individual chromophore units capable of absorbing light at different wavelengths.[12] They can exceptionally capture several photons over a broad region of the solar spectrum.[7,11,13−26] Because of their highly controllable synthesis that provides them with a specific architecture and high degree of order, they are suitable for a broad range of photoelectronic applications, such as light-emitting diodes, electronic sensors, and bio-organic and nanomedicine applications.[27,28]

The high efficiency of dendrimers to funnel harvested light to a localized site depends on how the different chromophore units are assembled in the supramolecular structure.[29−40] Dendrimers with built-in energy gradients require ordered structures wherein the chromophore units change their optical properties in specific, predefined spatial directions. Otherwise, photoexcitation leads to a spatial scrambling of the exciton among equivalent chromophore units.[41−43]

Among a wide variety of branched conjugated dendrimers,[44−46] the family of dendrimers, based on poly(phenylene−ethynylene) (PPE) units, originally introduced by Moore, Kopelman, and co-workers, has been the subject of extensive theoretical and experimental studies[39,47−50] because of their ability to mimic both the light harvesting and energy funneling that occur in photosynthetic systems.[32,44,46,51,52] Because they can be synthesized with high regularity and controlled molecular weights, as well as their potential for functionalization, PPE dendrimers offer great promise in the control of energy funneling.[10]

Previous studies performed on both types of PPE dendrimers provide qualitative pictures of the relationship between dendrimer topology and efficiency in energy funneling.[31,39,53,54] In this work, we computationally probe

Received: July 17, 2020
Revised: September 8, 2020
Published: September 28, 2020

the energy funneling mechanisms that occur after photoexcitation of the large, complex, unsymmetrical PPE dendrimer, denoted as $2G_2$m-EPer (Figure 1a). $2G_2$m-EPer

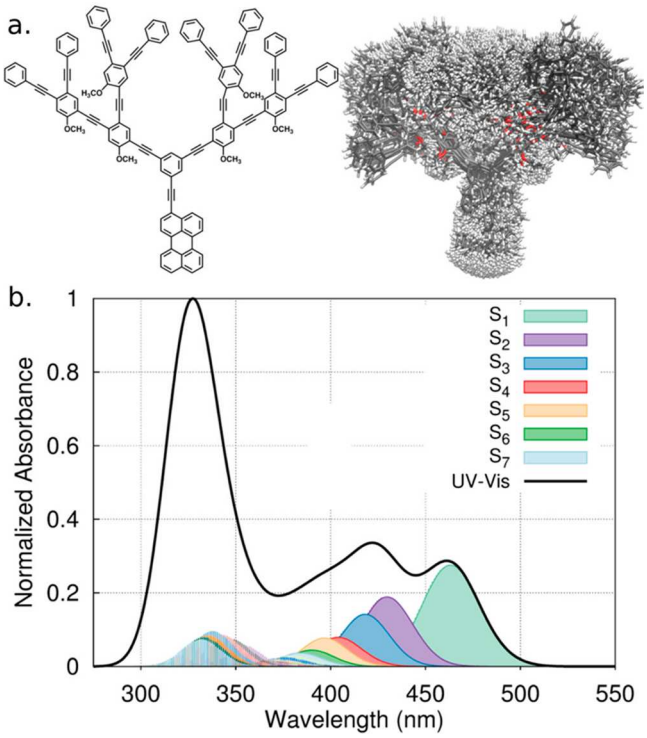

Figure 1. (a) Chemical structure of $2G_2$m-EPer (left). Superposition of 1000 snapshots of the structure obtained from ground state molecular dynamics demonstrating conformational diversity (right). (b) Simulated absorption spectra at 300 K showing contributions from the individual 30 excited states of each snapshot to the total spectrum.

is composed of two second-generation monodendrons linked through a phenylene−ethynylene unit by meta-substitution. The phenyl bridge is linked to an ethynylene−perylene trap (EPer). Each monodendron consists of phenylene−ethynylene (PE) subunits, branched by ortho-, meta-, and para-substitutions. While meta-substitutions localize the exciton in individual chromophore subunits, ortho- and para-substitutions allow for delocalization throughout the dendrimer backbone. That is meta-, ortho-, and para-branching between chromophore units modulate the optical and dynamic properties of the PPE dendrimer.[55] The ultimate pathways of energy funneling are subject to the intramolecular energy gradients created by their ordered combination within the dendrimer backbone.[30,53,56−58]

The photoinduced electronic energy relaxation and redistribution within $2G_2$m-EPer have been previously monitored by steady-state and time-resolved spectroscopies.[22,29,31,53,58,59] These studies have proposed a kinetic model for the highly efficient intramolecular energy funneling that takes place from the initial excited state on the didendron backbone to the EPer trap.[31] The model is based on two possible pathways, direct and indirect, for exciton migration toward the bottom of the energy funnel. While the direct (coherent) pathway involves direct exciton migration from the initial excited state (donor) to acceptor (EPer trap), the indirect (incoherent) pathway involves multistep exciton migration within the dendrimer backbone followed by the ultimate transfer to the EPer trap. Moreover, Kleiman et al. have shown that the emission quantum yield of $2G_2$m-EPer can be enhanced by 15% through the coherent control of its excited-state dynamics.[58] Computational insights are useful to fully understand these kinds of energy transfer mechanisms at an atomistic level and provide the excited state conformations.

In this work, the photoexcitation and subsequent energy relaxation and redistribution of $2G_2$m-EPer are simulated by using nonadiabatic excited state molecular dynamics (NEXMD). This methodology allows us to track the flow of the exciton between both monodendrons and the EPer trap; consequently, direct and indirect mechanisms of intramolecular energy funneling are distinguished and analyzed.

COMPUTATIONAL METHODS

The photoexcitation and subsequent intramolecular electronic energy funneling of $2G_2$m-EPer were simulated by using the NEXMD method.[43,60] NEXMD has been specifically developed to model photoinduced dynamics in large conjugated molecules involving multiple electronically coupled excited states. It makes use of the fewest switches surface hopping (FSSH) algorithm[61,62] with additional implementations to identify trivial unavoided crossings[63] and introduce electronic decoherence.[64] Excited state energies,[54,65] gradients,[66,67] and nonadiabatic couplings[43,54,68,69] were calculated "on the fly" by using the collective electronic oscillator (CEO) approach[54,54,65,70] at the configuration interaction singles (CIS) level of theory with the semiempirical Austin model 1 Hamiltonian (AM1).[71] Previous studies validate this level of theory to achieve a qualitative description of the photoinduced intramolecular energy flux in PPE dendrimers.[30,37−39,50,72] The details of the NEXMD approach, advantages, implementation, and testing parameters can be found elsewhere.[43,73−75]

The $2G_2$m-EPer geometry was initially optimized at the AM1 semiempirical level[71] by using Gaussian16.[76] After that, the molecule was heated from 0 to 300 K for 10 ps with an integration time step of 0.5 fs for the molecular dynamics by using the AMBER 18 program suite.[77] The GAFF (General Amber Force Field)[78,79] was used to parametrize the dendrimer, and a reparametrization of the dihedrals, which form among the C atoms of the aromatic ring and the C atoms of the triple bond, was performed with force constants of 0.40 kcal/mol. Finally, 5 ns of simulation was done at 300 K with a time step of 0.5 fs employing a Langevin thermostat with a friction coefficient of 20.0 ps^{-1}. One thousand snapshots were sample uniformly in time over the 5 ns molecular dynamics simulation. Each snapshot was further equilibrated by using quantum mechanics molecular dynamics, as it is implemented in AMBER 18, using the AM1 Hamiltonian during 3.5 ps to obtain the final initial sets of coordinates and momenta. For each of the stored configurations the first 30 excited states energies and oscillator strengths were computed by using the CEO approach to obtain the absorption spectrum.

To mimic the experimental setup, for each NEXMD simulation, the initial excited state was obtained by using a Franck−Condon window given by $g_\alpha = \exp[-(T/\hbar)^2(E_{laser} - \Omega_\alpha)^2]$, with Ω_α and E_{laser} representing the energy gap between the ground state and the αth excited state and the energy of a Gaussian laser pulse $f(t) = \exp(-t^2/2T^2)$ centered at 400 nm, respectively. Thus, the selection of the initial excited state was randomly according to the oscillator strengths of each α state and the values of g_α, where T has a value of 42.5 fs according to

https://dx.doi.org/10.1021/acs.jpcc.0c06539
J. Phys. Chem. C 2020, 124, 22383−22391

the laser full width at half-maximum of 100 fs. Each NEXMD simulation was run for 150 fs using a classical time step of 0.1 fs for nuclei propagation and a quantum time step of 0.025 fs for electronic degrees of freedom. Ten singlet electronic excited states and their corresponding nonadiabatic couplings were included.

RESULTS AND DISCUSSION

$2G_2$m-EPer is an unsymmetrical PPE dendrimer composed of three moieties (see Figure 1a): two individual monodendrons comprising the backbone structures connected to the core ring and the EPer unit. Meta-branching in the core ring breaks the π-electron conjugation in the ground electronic state, defining them as three individual, weakly coupled chromophores. The ground state conformational sampling at T = 300 K reveals a high degree of conformational diversity, represented in Figure 1a as a superposition of snapshots of the $2G_2$m-EPer structure obtained from equilibrated ground state molecular dynamics.

The simulated absorption spectrum of $2G_2$m-EPer is shown in Figure 1b. This spectrum was obtained as a convolution of the thousand individual spectra obtained from the ground state molecular dynamics; each spectrum is calculated by using the vertical transition energies and their corresponding oscillator strengths. The computed spectrum is red-shifted by ~30 nm with respect to experimental data reported by Kleiman et al.; however, it captures the key spectral features in the their report.[31] The contributions of the two lowest excited states overlap, with their maxima separated by around 34 ± 17 nm, in agreement with the experimental value of 39 nm. This spectral overlap is significantly larger with respect to the first-generation counterpart, $2G_1$m-Eper dendrimer.[50] In fact, the average energy difference between the S_2 and S_1 states at 0 fs of the nonadiabatic dynamics is 0.21 ± 0.10 and 0.41 ± 0.10 eV for $2G_2$m-EPer and $2G_1$m-Eper, respectively. Notably, the separation of these states for $2G_1$m-Eper is twice that of $2G_2$m-Eper.

The simulated single peak around 470 nm is associated with the $S_0 \rightarrow S_1$ transition, and it is comparable with the experimental band in the region between 430 and 500 nm.

Previous steady-state and time-resolved fluorescence measurements identify the two monodendrons and the EPer unit as the donors and acceptors, respectively, during the ultrafast intramolecular energy transfer that takes place after photoexcitation.[31] Analysis of the localization of the electronic transition density of the seven lowest electronic states at the minimum of the ground state potential energy surface (see Figure S1 in the Supporting Information) indicates that the S_1 state is completely localized at the EPer, while the S_1 state is completely localized at the acceptor EPer and the S_2−S_7 states are localized at the donor monodendrons. Therefore, the intramolecular donor → acceptor energy funneling can be followed by tracking the average populations of different electronic excited states as a function of time (Figure 2a). The laser photoexcitation at 400 nm, according to the initial excited state selection described in the Computational Methods section, creates an initial distribution of average populations on electronic excited states composed of 25%, 32%, 26%, and 11% of states S_5, S_6, S_7, and S_8, respectively. During the first ~20 fs after photoexcitation, these initially populated excited states experience an ultrafast energy relaxation, transferring their populations to the intermediate S_4 and S_3 states. By 120 fs, the transient accumulated populations in S_4 and S_3 states relax to S_2. Finally, an efficient, ultrafast transfer of population

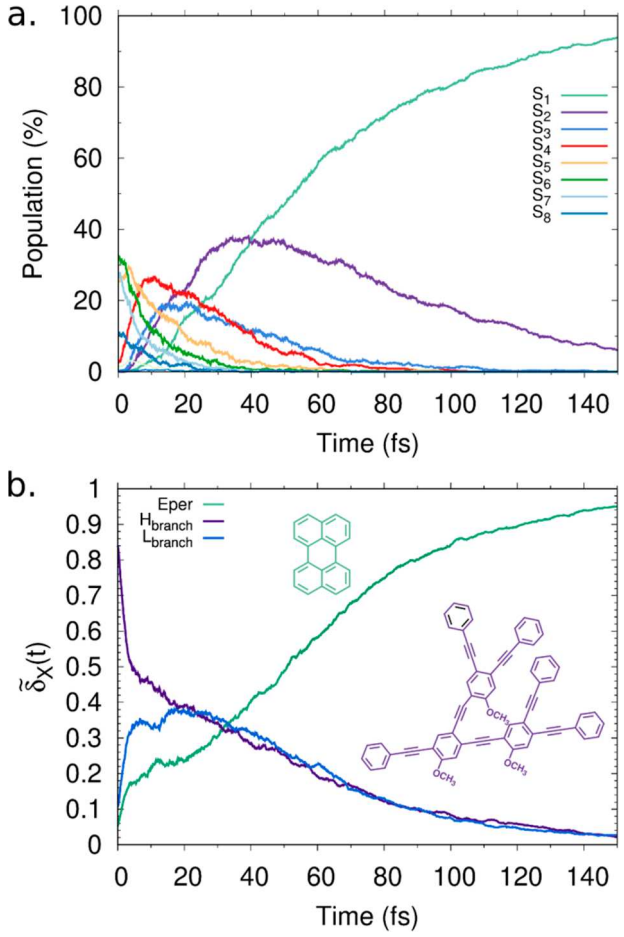

Figure 2. (a) Evolution in time of electronic state populations for 1000 trajectories. (b) Evolution in time of the partial average electronic transition density ($\tilde{\delta}_X(t)$) for the three moieties: the two monodendrons and the EPer unit.

to the S_1 state is achieved in ~150 fs. It is interesting to note that the observed ultrafast migration to the lowest S_1 state is significantly faster than the previously reported electronic energy relaxation for the corresponding smaller, first-generation unsymmetrical $2G_1$m-Eper dendrimer, whose simulated electronic relaxation takes place in ~500 fs.[50] A detailed comparison of the electronic energy relaxation for both dendrimers indicates that while high-energy excited states relax in ~100 fs in both cases, the S_2 state acts as the bottleneck in the sequential relaxation process of the $2G_1$m-Eper dendrimer. Figure 2a shows a transient accumulation of the S_2 population of ~40% for $2G_2$m-EPer, while the corresponding transient accumulation in $2G_1$m-Eper reaches values of up to 70% due to the aforementioned overlap between S_2 and S_1 states in $2G_2$m-EPer versus the greater separation of these states in the $2G_1$m-Eper dendrimer.[50]

Further characterization of the donor → acceptor energy funneling in $2G_2$m-EPer is done by analyzing the evolution of the spatial localization of the electronic transition density over time. In the CEO approach, the elements of the transition density matrices are written as

$$(\rho^{g\alpha})_{mn} = \langle \phi_\alpha | c_n^\dagger c_m | \phi_g \rangle \quad (1)$$

where c_m and $c_n^\dagger$ are the annihilation and creation operators of electrons for atomic orbitals n and m, respectively, and ϕ_α and

https://dx.doi.org/10.1021/acs.jpcc.0c06539
J. Phys. Chem. C 2020, 124, 22383−22391

ϕ_g represent the CIS adiabatic excited and ground state wave functions, respectively.[70,80] Diagonal elements represent the changes in the distribution of electronic density on the mth AO induced by the photoexcitation from the ground state to the singlet excited state S_α.[70,81] This property makes the transition density matrix useful for capturing the relaxation dynamics of the excited state wave functions in real space.

Considering the normalization condition $\sum_{n,m}(\rho^{g\alpha}_{nm}(t))^2 = 1$, the fraction of the transition density localized on each of the three moieties, that is, the two monodendrons (donors) and the EPer unit (acceptor), is obtained as

$$\delta^{\alpha}_{X}(t) = (\rho^{g\alpha}(t))_X{}^2 = \sum_{n_A m_A} (\rho^{g\alpha}(t))_{n_A m_A}{}^2 \quad (2)$$

where the index A runs over all atoms localized in the moiety X.[65]

Figure 2b shows the evolution of $\tilde{\delta}_X(t)$ for the three moieties of 2G$_2$m-EPer over time, where $\tilde{\delta}_X(t) = \langle \sum_{\alpha=1}^{8} P_\alpha(t)\delta^{\alpha}_{X}(t)\rangle$, with $P_\alpha(t)$ the population of excited state α during the FSSH trajectory, and the angle brackets correspond to an average over the ensemble of FSSH trajectories. The initial exciton localization on both monodendrons is transferred to the EPer trap, confirming the highly efficient intramolecular donor → acceptor energy funneling proposed by previous experimental studies.[15] The kinetics followed by $\delta^{\alpha}_{\mathrm{EPer}}(t)$ follows the increase of S$_1$ population shown in Figure 2a, indicating that this state remains localized on the EPer unit throughout the relaxation process. To analyze the evolution of the average transition density localized in each monodendron for each NEXMD trajectory, we differentiate the monodendron units based on the transition density localization after the excitation.

Further analysis of the intramolecular energy redistribution following the initial photoexcitation of 2G$_2$m-EPer can be achieved by applying the transition density flux method.[82] Briefly, during each time interval Δt, throughout the NEXMD simulations, the effective change in the partial electronic transition density ($\Delta\delta_X(t) = \delta_X(t + \Delta t) - \delta_X(t)$, where we have dropped the electronic state index for notational simplicity) is monitored by calculating the flow matrix $F(t)$. While diagonal elements $F(t)$ are zero, off-diagonal elements $f_{XY}(t)$ contain the amount of $\delta_X(t)$ transferred between units X and Y. By classifying chromophore units as donors (D) if $\Delta\delta_X(t) < 0$ or acceptors (A) if $\Delta\delta X(t) > 0$ and imposing the minimum flow criterion, we can calculate flow matrix elements between two units ($f_{YX}(t)$) as

$$\frac{|\Delta\delta_X(t)|\Delta\delta_Y(t)}{\Delta\delta_{\mathrm{total}}(t)} \quad (3)$$

with

$$\Delta\delta_{\mathrm{total}}(t) = |\sum \Delta\delta_X(t)| = \sum \Delta\delta_Y(t) \quad (4)$$

These new matrixes represent the accumulated flux between two chromophore units; matrix values are positive over time when moving from donor to acceptor and negative in the opposite case: $f_{XY}(t) = -f_{YX}(t)$. More details about the transition density flux method can be found elsewhere.[82]

Figures 4a–c show the average accumulated fluxes for the three chromophore units of 2G$_2$m-EPer, where we observe energy transfer from both monodendrons to the acceptor EPer trap. At earlier times in the dynamics, an ultrafast direct monodendron H → Eper energy transfer is observed. This is not the case for the monodendron L → Eper transfer that experiences a delay of ∼20 fs. After that, transfer from both monodendrons to the Eper trap seems to follow similar kinetics. Figure 4b reveals that during the ultrafast direct initial monodendron H → Eper energy transfer a monodendron H → monodendron L energy flux also occurs. According to Figure 4c, monodendron H acts mainly as a donor unit, except at times ∼10 fs when a small, transient energetic feedback from monodendron L to monodendron H seems to take place.

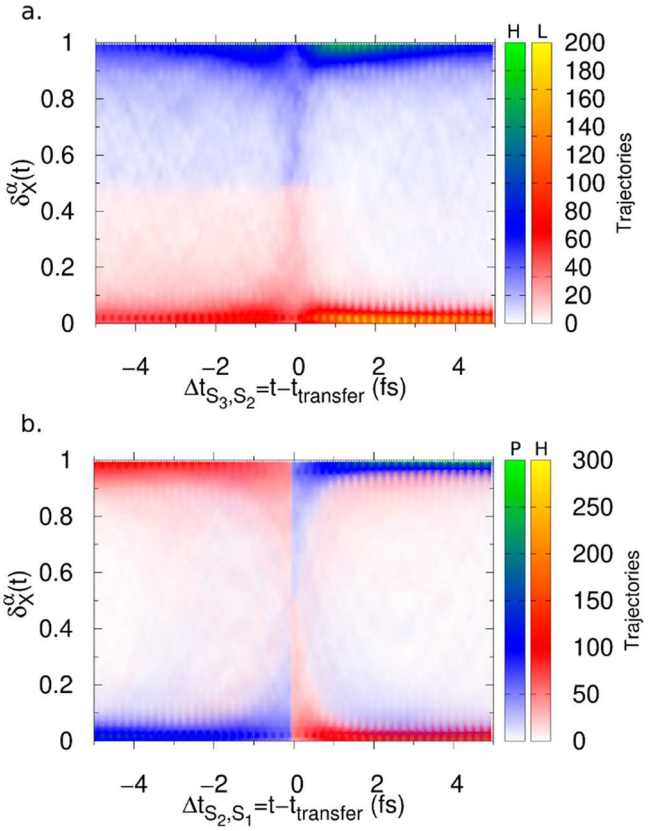

Figure 3. (a) $\delta^{\alpha}_{X}(t)$ distribution around the S$_3$ → S$_2$ transition. The blue-green color corresponds to H-monodendron moiety, and the red-yellow color corresponds to L-monodendron moiety. Before the transition, the $\delta^{\alpha}_{X}(t)$ contour distribution shows delocalization in both monodendrons; after the transition the $\delta^{\alpha}_{X}(t)$ contour distribution is mainly localized in the H moiety. (b) $\delta^{\alpha}_{X}(t)$ distribution around the S$_2$ → S$_1$ transition. The distribution is localized on the H monodendron before the S$_2$ → S$_1$ transition, and it is localized on the perylene after the hop. H: high-density monodendron; L: low-density monodendron; P: perylene.

These results suggest a fast energy exchange between the two monodendrons before the final transfer to the perylene in agreement with the data shown in Figure 2b.

In the context of previous steady-state spectroscopy and time-resolved fluorescence measurements,[31] the above results allow us to conceptualize two potential energy transfer pathways: direct and indirect. Further inspection of potential mechanisms can be achieved by analyzing the distribution of the lapses in time during which the system is localized in the S$_2$ state, that is, the time during which the S$_2$ state corresponds to the current state according the FSSH prescription. This is shown in Figure 5a when the distribution of the elapsed times in the S$_2$ states exhibits at least two different pathways. We assign trajectories that spend less than 10 fs in the S$_2$ state before the ultimate transfer to the S$_1$ state localized on the

https://dx.doi.org/10.1021/acs.jpcc.0c06539
J. Phys. Chem. C 2020, 124, 22383−22391

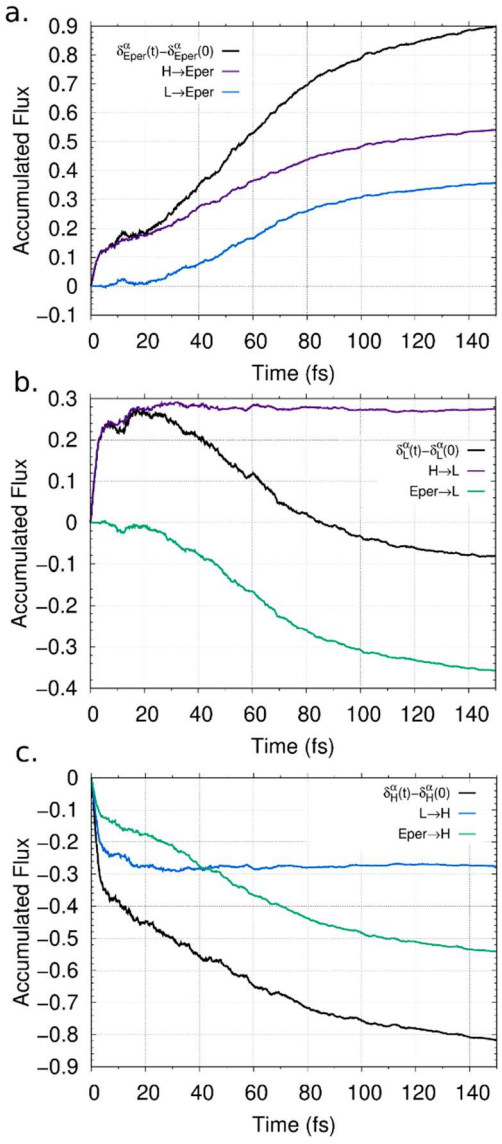

Figure 4. (a) Average accumulated flux for Eper unit computed by using the transition density flux method. (b) Average accumulated flux for monodendron L computed by using the transition density flux method. (c) Average accumulated flu for monodendron H computed by using the transition density flux method.

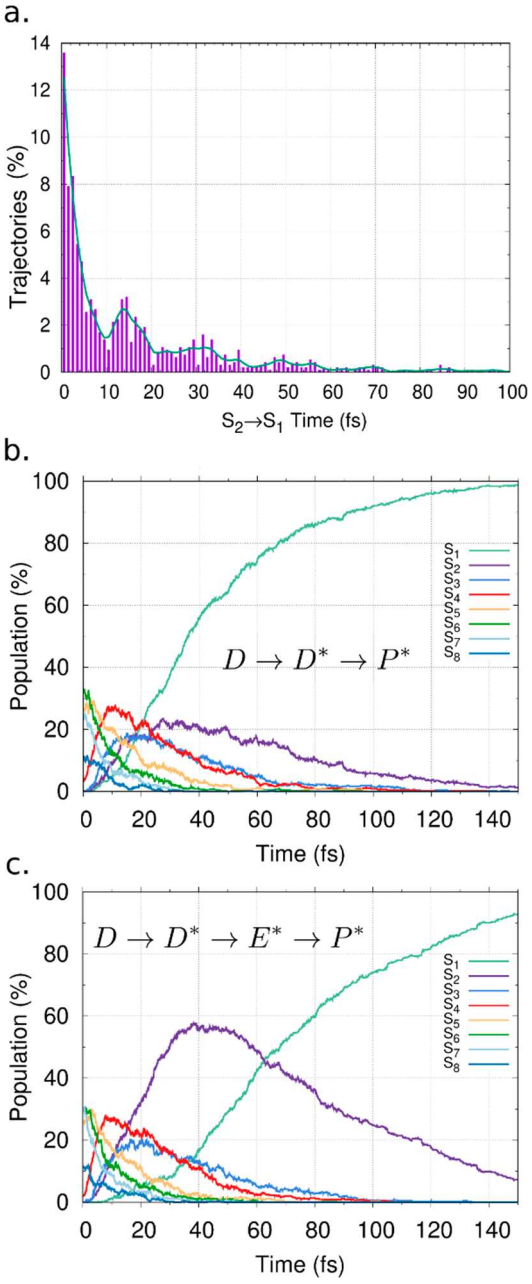

Figure 5. (a) Time distribution of the trajectories in the S_2 state before jumping to S_1. (b) Population distribution in each excited state over time for dynamics classified as direct mechanism. (c) Population distribution in each excited state over time for dynamics classified as indirect mechanism.

EPer trap to follow the direct transfer pathway. On the other hand, a second type of trajectory follows the indirect pathway, where the exciton is transiently localized in S_2 for longer than 10 fs. Figures 6a,b summarize these findings (to be consistent with previous experimental proposal by Kleiman et al., the same nomenclature is used in our mechanistic assignments).[31]

Direct Mechanism. $D \rightarrow D^* \rightarrow E^* \rightarrow P^* \rightarrow$ *Emission*: After the initial $D \rightarrow D^*$ photoexcitation, excited states D^* are mainly localized on the donor monodendrons ($\geq S_3$). The exciton experiences an ultrafast exchange between these high-energy states involving different degrees of delocalization between both H and L monodendrons (see Figure S1). According to Figures 4b,c (H → L), the exciton exchange between monodendrons is limited to the first ~40 fs. Finally, the energy is transferred to the state P^* localized on the EPer trap without being self-trapped in any of the two monodendrons for more than 10 fs.

Indirect Mechanism. $D \rightarrow D^* \rightarrow E^* \rightarrow P^* \rightarrow$ *Emission*: This mechanism has the same initial and final excited states as the aforementioned direct case. However, in this pathway, the exciton is transiently self-trapped in the S_2 state, represented as E^*, for times longer than 10 fs. According to the spatial localization of the electronic transition density in that state, the exciton will remain self-trapped on one monodendron.

To analyze the two different energy transfer pathways, we can separate distinct bundles of trajectories according to the elapsed time in the S_2 state. Figures 5b and 5c display the evolution over time of electronic state populations for trajectories that follow the direct or indirect mechanism, respectively, that is, trajectories in which the exciton is

https://dx.doi.org/10.1021/acs.jpcc.0c06539
J. Phys. Chem. C 2020, 124, 22383−22391

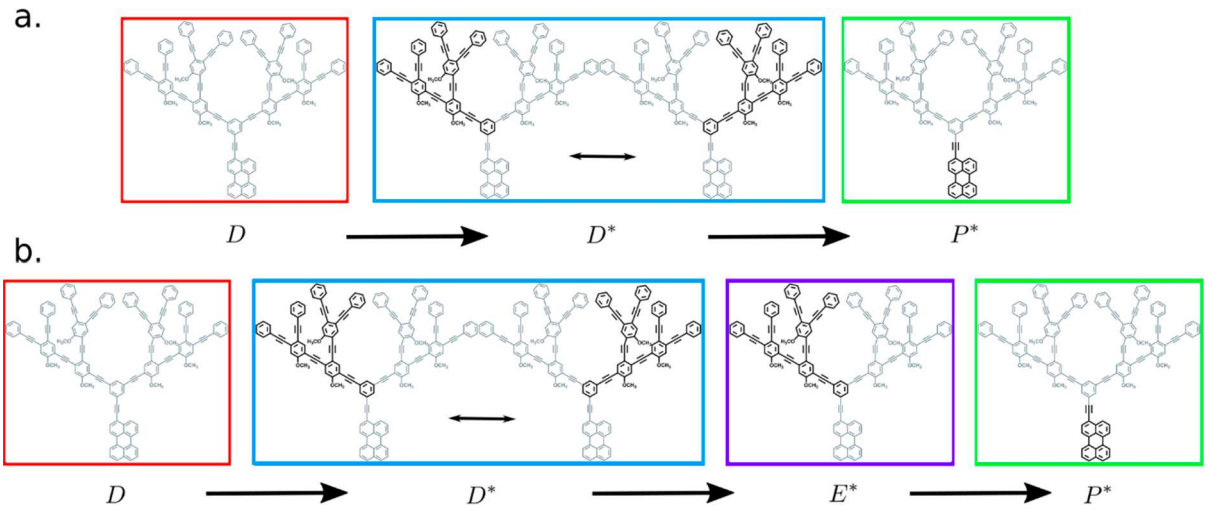

Figure 6. Schematic representation of the (a) direct and (b) indirect energy transfer pathways.

transiently self-trapped in the S_2 state for times shorter or longer than 10 fs, respectively. Overall, we found that 51% of trajectories follow the direct mechanism, while 49% follow the indirect mechanism of intramolecular energy transfer after photoexcitation at 400 nm, which can be compared with an excitation at 370 nm done. Our results are in good agreement with previously reported time-resolved fluorescence measurements which reveal 54% and 46% contributions from direct and indirect pathways, respectively, after excitation at 340 nm and 36% and 64% after excitation at 380 nm.[31] That is, the relative contribution of the indirect pathways increases with the increase of the wavelength of the initial laser excitation. Comparison of Figures 5b and 5c indicates similar time dependencies for the electronic populations of the initial excited states (S_n, $n \geq 3$) in both mechanisms. The two mechanisms differ in the lifetime of the S_2 state and, ultimately, the transition time to S_1. In other words, the transient exciton self-trapping on one monodendron slows down the intramolecular donor → acceptor energy funneling.

CONCLUSIONS

Our simulations of the nonradiative photoinduced energy relaxation and redistribution of $2G_2$m-EPer allow us to track the flow of electronic transition density between both monodendrons (donors) and the EPer trap (acceptor), confirming the unidirectional donor → acceptor energy transfer. We also explore the contributions of the different mechanisms responsible for its highly efficient energy funneling. In this way, the two possible direct and indirect pathways for exciton migrations, previously reported by time-resolved spectroscopy, are rigorously defined. In both the direct and indirect mechanisms, the exciton initially experiences an ultrafast exchange between high-energy states (S_n, $n \geq 3$) involving different degrees of delocalization between both monodendrons. After that, the two mechanisms differ from each other by the exciton self-trapping on the S_2 state observed in the indirect mechanism, that is, the transient exciton spatial localization on one monodendron. In this way, the contribution of the indirect mechanism slows down the intramolecular donor → acceptor energy funneling, potentially stimulating energy dissipation. Our simulations can contribute to future developments of new classes of dendrimers for applications in molecular-based photonics devices as we have shown that enhancements in the photoemission efficiency can be predicted by optimizing the relative contributions of the different intramolecular energy transfer pathways.

ASSOCIATED CONTENT

Supporting Information

The Supporting Information is available free of charge at https://pubs.acs.org/doi/10.1021/acs.jpcc.0c06539.

Figure S1: the transition density matrices in an orbital representation for S_1 to S_8 states (PDF)

AUTHOR INFORMATION

Corresponding Author

Johan F. Galindo − *Department of Chemistry, Universidad Nacional de Colombia, Bogotá 111321, Colombia;* orcid.org/0000-0001-9968-362X; Email: jfgalindoc@unal.edu.co

Authors

Maria Camila Aguilera − *Department of Chemistry, Universidad Nacional de Colombia, Bogotá 111321, Colombia*

Adrian E. Roitberg − *Department of Chemistry, University of Florida, Gainesville, Florida 32611, United States;* orcid.org/0000-0003-3963-8784

Valeria D. Kleiman − *Department of Chemistry, University of Florida, Gainesville, Florida 32611, United States;* orcid.org/0000-0002-9975-6558

Sebastian Fernandez-Alberti − *Universidad Nacional de Quilmes/CONICET, Bernal B1876BXD, Argentina;* orcid.org/0000-0002-0916-5069

Complete contact information is available at: https://pubs.acs.org/10.1021/acs.jpcc.0c06539

Notes

The authors declare no competing financial interest.

ACKNOWLEDGMENTS

The authors thank Dr. Sergei Tretiak at Los Alamos National Lab for providing computational resources and support during the development of this work. S.F.-A. acknowledges support of CONICET, UNQ, and ANPCyT (PICT-2018-02360). J.F.G. thanks DIEB-UNAL for financial support. V.D.K. acknowl-

edges financial support from the National Science Foundation (CHE-1802240).

REFERENCES

(1) Andrews, D. L. Light Harvesting in Dendrimer Materials: Designer Photophysics and Electrodynamics. *J. Mater. Res.* **2012**, *27*, 627−638.

(2) Adronov, A.; Fréchet, J. M. J. Light-Harvesting Dendrimers. *Chem. Commun.* **2000**, *18*, 1701−1710.

(3) Cox, M.; Nelson, D. *Lehninger Principles of Biochemistry*; W.H. Freeman: New York, 2008; Vol. *5*.

(4) Hu, X.; Damjanović, A.; Ritz, T.; Schulten, K. Architecture and Mechanism of the Light-Harvesting Apparatus of Purple Bacteria. *Proc. Natl. Acad. Sci. U. S. A.* **1998**, *95*, 5935−5941.

(5) Caycedo-Soler, F.; Rodríguez, F. J.; Quiroga, L.; Johnson, N. F. Light-Harvesting Mechanism of Bacteria Exploits a Critical Interplay between the Dynamics of Transport and Trapping. *Phys. Rev. Lett.* **2010**, *104*, 158302−158302−4.

(6) Engel, G. S.; Calhoun, T. R.; Read, E. L.; Ahn, T.-K.; Mančal, T.; Cheng, Y.-C.; Blankenship, R. E.; Fleming, G. R. Evidence for Wavelike Energy Transfer through Quantum Coherence in Photosynthetic Systems. *Nature* **2007**, *446*, 782−786.

(7) Gilat, S. L.; Adronov, A.; Fréchet, J. M. J. Light Harvesting and Energy Transfer in Novel Convergently Constructed Dendrimers. *Angew. Chem., Int. Ed.* **1999**, *38*, 1422−1427.

(8) Adronov, A.; Robello, D. R.; Fréchet, J. M. J. Light Harvesting and Energy Transfer within Coumarin-Labeled Polymers. *J. Polym. Sci., Part A: Polym. Chem.* **2001**, *39*, 1366−1373.

(9) Kozaki, M.; Suzuki, S.; Okada, K. Dendritic Light-Harvesting Antennas with Excitation Energy Gradients. *Chem. Lett.* **2013**, *42*, 1112−1118.

(10) Inoue, K. Functional Dendrimers, Hyperbranched and Star Polymers. *Prog. Polym. Sci.* **2000**, *25*, 453−571.

(11) Devadoss, C.; Bharathi, P.; Moore, J. S. Energy Transfer in Dendritic Macromolecules: Molecular Size Effects and the Role of an Energy Gradient. *J. Am. Chem. Soc.* **1996**, *118*, 9635−9644.

(12) Sowinska, M.; Urbanczyk-Lipkowska, Z. Advances in the Chemistry of Dendrimers. *New J. Chem.* **2014**, *38*, 2168−2203.

(13) Fréchet, J. M. J.; Tomalia, D. A. *Dendrimers and Other Dendritic Polymers*; John Wiley & Sons, Ltd.: West Sussex, UK, 2001.

(14) Frischmann, P. D.; Mahata, K.; Würthner, F. Powering the Future of Molecular Artificial Photosynthesis with Light-Harvesting Metallosupramolecular Dye Assemblies. *Chem. Soc. Rev.* **2013**, *42*, 1847−1870.

(15) Tomalia, D. A.; Baker, H.; Dewald, J.; Hall, M.; Kallos, G.; Martin, S.; Roeck, J.; Ryder, J.; Smith, P. Dendritic Macromolecules: Synthesis of Starburst Dendrimers. *Macromolecules* **1986**, *19*, 2466−2468.

(16) Newkome, G. R.; Yao, Z.; Baker, G. R.; Gupta, V. K. Micelles. Part 1. Cascade Molecules: A New Approach to Micelles. A [27]-Arborol. *J. Org. Chem.* **1985**, *50*, 2003−2004.

(17) Fréchet, J. M. J. Dendrimers and Supramolecular Chemistry. *Proc. Natl. Acad. Sci. U. S. A.* **2002**, *99*, 4782−4787.

(18) Fréchet, J. M. J. Dendrimers and Other Dendritic Macromolecules: From Building Blocks to Functional Assemblies in Nanoscience and Nanotechnology. *J. Polym. Sci., Part A: Polym. Chem.* **2003**, *41*, 3713−3725.

(19) Rajakumar, P.; Kalpana, V.; Ganesan, S.; Maruthamuthu, P. Synthesis of Benzothiazole−Benzoxazole Dendrimers with Triazole as Bridging Unit and Their Application in Dye-Sensitized Solar Cells. *New J. Chem.* **2013**, *37*, 3692−3700.

(20) Froehling, P. E. Dendrimers and Dyes — a Review. *Dyes Pigm.* **2001**, *48*, 187−195.

(21) Denti, G.; Campagna, S.; Serroni, S.; Ciano, M.; Balzani, V. Decanuclear Homo- and Heterometallic Polypyridine Complexes: Syntheses, Absorption Spectra, Luminescence, Electrochemical Oxidation, and Intercomponent Energy Transfer. *J. Am. Chem. Soc.* **1992**, *114*, 2944−2950.

(22) Peng, Z.; Melinger, J. S.; Kleiman, V. Light Harvesting Unsymmetrical Conjugated Dendrimders as Photosynthetic Mimics. *Photosynth. Res.* **2006**, *87*, 115−131.

(23) Bosman, A. W.; Janssen, H. M.; Meijer, E. W. About Dendrimers: Structure, Physical Properties, and Applications. *Chem. Rev.* **1999**, *99*, 1665−1688.

(24) Balzani, V.; Ceroni, P.; Maestri, M.; Vicinelli, V. Light-Harvesting Dendrimers. *Curr. Opin. Chem. Biol.* **2003**, *7*, 657−665.

(25) Nantalaksakul, A.; Reddy, D. R.; Bardeen, C. J.; Thayumanavan, S. Light Harvesting Dendrimers. *Photosynth. Res.* **2006**, *87*, 133−150.

(26) Balzani, V.; Credi, A.; Venturi, M. *Molecular Devices and Machines: Concepts and Perspectives for the Nanoworld*, 3rd ed.; Wiley-VCH Verlag GmbH & Co. KGaA: Weinheim, 2008.

(27) Kim, Y.; Zimmerman, S. C. Applications of Dendrimers in Bio-Organic Chemistry. *Curr. Opin. Chem. Biol.* **1998**, *2*, 733−742.

(28) Astruc, D.; Boisselier, E.; Ornelas, C. Dendrimers Designed for Functions: From Physical, Photophysical, and Supramolecular Properties to Applications in Sensing, Catalysis, Molecular Electronics, Photonics, and Nanomedicine. *Chem. Rev.* **2010**, *110*, 1857−1959.

(29) Kleiman, V. D.; Melinger, J. S.; McMorrow, D. Ultrafast Dynamics of Electronic Excitations in a Light-Harvesting Phenylacetylene Dendrimer. *J. Phys. Chem. B* **2001**, *105*, 5595−5598.

(30) Fernandez-Alberti, S.; Kleiman, V. D.; Tretiak, S.; Roitberg, A. E. Unidirectional Energy Transfer in Conjugated Molecules: The Crucial Role of High-Frequency C≡C Bonds. *J. Phys. Chem. Lett.* **2010**, *1*, 2699−2704.

(31) Atas, E.; Peng, Z.; Kleiman, V. D. Energy Transfer in Unsymmetrical Phenylene Ethynylene Dendrimers. *J. Phys. Chem. B* **2005**, *109*, 13553−13560.

(32) Swallen, S. F.; Kopelman, R.; Moore, J. S.; Devadoss, C. Dendrimer Photoantenna Supermolecules: Energetic Funnels, Exciton Hopping and Correlated Excimer Formation. *J. Mol. Struct.* **1999**, *485−486*, 585−597.

(33) Rana, D.; Gangopadhyay, G. Studies on Energy Transfer in Dendrimer Supermolecule Using Classical Random Walk Model and Eyring Model. *J. Chem. Phys.* **2003**, *118*, 434−443.

(34) Raychaudhuri, S.; Shapir, Y.; Mukamel, S. Disorder and Funneling Effects on Exciton Migration in Treelike Dendrimers. *Phys. Rev. E: Stat. Phys., Plasmas, Fluids, Relat. Interdiscip. Top.* **2002**, *65*, 021803−021803−12.

(35) Martín-Delgado, M. A.; Rodriguez-Laguna, J.; Sierra, G. Density-Matrix Renormalization-Group Study of Excitons in Dendrimers. *Phys. Rev. B: Condens. Matter Mater. Phys.* **2002**, *65*, 155116−155116−11.

(36) Bar-Haim, A.; Klafter, J.; Kopelman, R. Dendrimers as Controlled Artificial Energy Antennae. *J. Am. Chem. Soc.* **1997**, *119*, 6197−6198.

(37) Ondarse-Alvarez, D.; Kömürlü, S.; Roitberg, A. E.; Pierdominici-Sottile, G.; Tretiak, S.; Fernandez-Alberti, S.; Kleiman, V. D. Ultrafast Electronic Energy Relaxation in a Conjugated Dendrimer Leading to Inter-Branch Energy Redistribution. *Phys. Chem. Chem. Phys.* **2016**, *18*, 25080−25089.

(38) Fernandez-Alberti, S.; Kleiman, V. D.; Tretiak, S.; Roitberg, A. E. Nonadiabatic Molecular Dynamics Simulations of the Energy Transfer between Building Blocks in a Phenylene Ethynylene Dendrimer. *J. Phys. Chem. A* **2009**, *113*, 7535−7542.

(39) Fernandez-Alberti, S.; Roitberg, A. E.; Kleiman, V. D.; Nelson, T.; Tretiak, S. Shishiodoshi Unidirectional Energy Transfer Mechanism in Phenylene Ethynylene Dendrimers. *J. Chem. Phys.* **2012**, *137*, 22A526−22A526−9.

(40) Liu, J.; Thiel, W. An Efficient Implementation of Semiempirical Quantum-Chemical Orthogonalization-Corrected Methods for Excited-State Dynamics. *J. Chem. Phys.* **2018**, *148*, 154103.

(41) Bradshaw, D. S.; Andrews, D. L. Mechanisms of Light Energy Harvesting in Dendrimers and Hyperbranched Polymers. *Polymers* **2011**, *3*, 2053−2077.

https://dx.doi.org/10.1021/acs.jpcc.0c06539
J. Phys. Chem. C 2020, 124, 22383−22391

(42) Nelson, T. R.; Ondarse-Alvarez, D.; Oldani, N.; Rodriguez-Hernandez, B.; Alfonso-Hernandez, L.; Galindo, J. F.; Kleiman, V. D.; Fernandez-Alberti, S.; Roitberg, A. E.; Tretiak, S. Coherent Exciton-Vibrational Dynamics and Energy Transfer in Conjugated Organics. *Nat. Commun.* **2018**, *9*, 2316.
(43) Nelson, T.; Fernandez-Alberti, S.; Roitberg, A. E.; Tretiak, S. Nonadiabatic Excited-State Molecular Dynamics: Modeling Photophysics in Organic Conjugated Materials. *Acc. Chem. Res.* **2014**, *47*, 1155−1164.
(44) Rana, D.; Gangopadhyay, G. Steady-State Spectral Properties of Dendrimer Supermolecule as a Light Harvesting System. *Chem. Phys. Lett.* **2001**, *334*, 314−324.
(45) Vögtle, F.; Gorka, M.; Hesse, R.; Ceroni, P.; Maestri, M.; Balzani, V. Photochemical and Photophysical Properties of Poly-(Propylene Amine) Dendrimers with Peripheral Naphthalene and Azobenzene Groups. *Photochem. Photobiol. Sci.* **2002**, *1*, 45−51.
(46) Frechet, J. M. Functional Polymers and Dendrimers: Reactivity, Molecular Architecture, and Interfacial Energy. *Science* **1994**, *263*, 1710−1715.
(47) Shortreed, M. R.; Swallen, S. F.; Shi, Z.-Y.; Tan, W.; Xu, Z.; Devadoss, C.; Moore, J. S.; Kopelman, R. Directed Energy Transfer Funnels in Dendrimeric Antenna Supermolecules†. *J. Phys. Chem. B* **1997**, *101*, 6318−6322.
(48) Egbe, D. A. M.; Roll, C. P.; Klemm, E. Synthesis, Characterisation and Properties of Highly Luminescent and Liquid-Crystalline Alternating PPE/PPV-Copolymers. *Des. Monomers Polym.* **2002**, *5*, 245−275.
(49) Xu, Z.; Kahr, M.; Walker, K. L.; Wilkins, C. L.; Moore, J. S. Phenylacetylene Dendrimers by the Divergent, Convergent, and Double-Stage Convergent Methods. *J. Am. Chem. Soc.* **1994**, *116*, 4537−4550.
(50) Galindo, J. F.; Atas, E.; Altan, A.; Kuroda, D. G.; Fernandez-Alberti, S.; Tretiak, S.; Roitberg, A. E.; Kleiman, V. D. Dynamics of Energy Transfer in a Conjugated Dendrimer Driven by Ultrafast Localization of Excitations. *J. Am. Chem. Soc.* **2015**, *137*, 11637−11644.
(51) Kopelman, R.; Shortreed, M.; Shi, Z. Y.; Tan, W.; Xu, Z.; Moore, J. S.; Bar-Haim, A.; Klafter, J. Spectroscopic Evidence for Excitonic Localization in Fractal Antenna Supermolecules. *Phys. Rev. Lett.* **1997**, *78*, 1239−1242.
(52) Swallen, S. F.; Zhu, Z.; Moore, J. S.; Kopelman, R. Correlated Excimer Formation and Molecular Rotational Dynamics in Phenylacetylene Dendrimers. *J. Phys. Chem. B* **2000**, *104*, 3988−3995.
(53) Melinger, J. S.; Pan, Y.; Kleiman, V. D.; Peng, Z.; Davis, B. L.; McMorrow, D.; Lu, M. Optical and Photophysical Properties of Light-Harvesting Phenylacetylene Monodendrons Based on Unsymmetrical Branching. *J. Am. Chem. Soc.* **2002**, *124*, 12002−12012.
(54) Tretiak, S.; Mukamel, S. Density Matrix Analysis and Simulation of Electronic Excitations in Conjugated and Aggregated Molecules. *Chem. Rev.* **2002**, *102*, 3171−3212.
(55) Xu, Z.; Moore, J. S. Design and Synthesis of a Convergent and Directional Molecular Antenna. *Acta Polym.* **1994**, *45*, 83−87.
(56) Ortiz, W.; Krueger, B. P.; Kleiman, V. D.; Krause, J. L.; Roitberg, A. E. Energy Transfer in the Nanostar: The Role of Coulombic Coupling and Dynamics. *J. Phys. Chem. B* **2005**, *109*, 11512−11519.
(57) Palma, J. L.; Atas, E.; Hardison, L.; Marder, T. B.; Collings, J. C.; Beeby, A.; Melinger, J. S.; Krause, J. L.; Kleiman, V. D.; Roitberg, A. E. Electronic Spectra of the Nanostar Dendrimer: Theory and Experiment. *J. Phys. Chem. C* **2010**, *114*, 20702−20712.
(58) Kuroda, D. G.; Singh, C. P.; Peng, Z.; Kleiman, V. D. Mapping Excited-State Dynamics by Coherent Control of a Dendrimer's Photoemission Efficiency. *Science* **2009**, *326*, 263−267.
(59) Pan, Y.; Lu, M.; Peng, Z.; Melinger, J. S. Synthesis and Optical Properties of Unsymmetrical Conjugated Dendrimers Focally Anchored with Perylenes in Different Geometries. *J. Org. Chem.* **2003**, *68*, 6952−6958.
(60) Sifain, A. E.; Bjorgaard, J. A.; Nelson, T. R.; Nebgen, B. T.; White, A. J.; Gifford, B. J.; Gao, D. W.; Prezhdo, O. V.; Fernandez-Alberti, S.; Roitberg, A. E.; Tretiak, S. Photoexcited Nonadiabatic Dynamics of Solvated Push−Pull π-Conjugated Oligomers with the NEXMD Software. *J. Chem. Theory Comput.* **2018**, *14*, 3955−3966.
(61) Tully, J. C. Molecular Dynamics with Electronic Transitions. *J. Chem. Phys.* **1990**, *93*, 1061−1071.
(62) Hammes-Schiffer, S.; Tully, J. C. Proton Transfer in Solution: Molecular Dynamics with Quantum Transitions. *J. Chem. Phys.* **1994**, *101*, 4657−4667.
(63) Fernandez-Alberti, S.; Roitberg, A. E.; Nelson, T.; Tretiak, S. Identification of Unavoided Crossings in Nonadiabatic Photoexcited Dynamics Involving Multiple Electronic States in Polyatomic Conjugated Molecules. *J. Chem. Phys.* **2012**, *137*, 014512−014512−10.
(64) Nelson, T.; Fernandez-Alberti, S.; Roitberg, A. E.; Tretiak, S. Nonadiabatic Excited-State Molecular Dynamics: Treatment of Electronic Decoherence. *J. Chem. Phys.* **2013**, *138*, 224111−2214111−13.
(65) Tretiak, S.; Isborn, C. M.; Niklasson, A. M. N.; Challacombe, M. Representation Independent Algorithms for Molecular Response Calculations in Time-Dependent Self-Consistent Field Theories. *J. Chem. Phys.* **2009**, *130*, 054111−054111−16.
(66) Furche, F.; Ahlrichs, R. Adiabatic Time-Dependent Density Functional Methods for Excited State Properties. *J. Chem. Phys.* **2002**, *117*, 7433−7447.
(67) Tretiak, S.; Chernyak, V. Resonant Nonlinear Polarizabilities in the Time-Dependent Density Functional Theory. *J. Chem. Phys.* **2003**, *119*, 8809−8823.
(68) Chernyak, V.; Mukamel, S. Density-Matrix Representation of Nonadiabatic Couplings in Time-Dependent Density Functional (TDDFT) Theories. *J. Chem. Phys.* **2000**, *112*, 3572−3579.
(69) Send, R.; Furche, F. First-Order Nonadiabatic Couplings from Time-Dependent Hybrid Density Functional Response Theory: Consistent Formalism, Implementation, and Performance. *J. Chem. Phys.* **2010**, *132*, 044107−044107−12.
(70) Tretiak, S.; Chernyak, V.; Mukamel, S. Two-Dimensional Real-Space Analysis of Optical Excitations in Acceptor-Substituted Carotenoids. *J. Am. Chem. Soc.* **1997**, *119*, 11408−11419.
(71) Dewar, M. J. S.; Zoebisch, E. G.; Healy, E. F.; Stewart, J. J. P. Development and Use of Quantum Mechanical Molecular Models. 76. AM1: A New General Purpose Quantum Mechanical Molecular Model. *J. Am. Chem. Soc.* **1985**, *107*, 3902−3909.
(72) Nelson, T. R.; White, A. J.; Bjorgaard, J. A.; Sifain, A. E.; Zhang, Y.; Nebgen, B.; Fernandez-Alberti, S.; Mozyrsky, D.; Roitberg, A. E.; Tretiak, S. Non-Adiabatic Excited-State Molecular Dynamics: Theory and Applications for Modeling Photophysics in Extended Molecular Materials. *Chem. Rev.* **2020**, *120*, 2215−2287.
(73) Nelson, T.; Fernandez-Alberti, S.; Chernyak, V.; Roitberg, A. E.; Tretiak, S. Nonadiabatic Excited-State Molecular Dynamics Modeling of Photoinduced Dynamics in Conjugated Molecules. *J. Phys. Chem. B* **2011**, *115*, 5402−5414.
(74) Nelson, T.; Fernandez-Alberti, S.; Chernyak, V.; Roitberg, A. E.; Tretiak, S. Nonadiabatic Excited-State Molecular Dynamics: Numerical Tests of Convergence and Parameters. *J. Chem. Phys.* **2012**, *136*, 054108−054108−12.
(75) Galindo, J. F.; Fernandez-Alberti, S.; Roitberg, A. E. Electronic Excited State Specific IR Spectra for Phenylene Ethynylene Dendrimer Building Blocks. *J. Phys. Chem. C* **2013**, *117*, 26517−26528.
(76) Frisch, M. J.; Trucks, G. W.; Schlegel, H. B.; Scuseria, G. E.; Robb, M. A.; Cheeseman, J. R.; Scalmani, G.; Barone, V.; Petersson, G. A.; Nakatsuji, H.; et al. *Gaussian 16*, revision C.01; Gaussian Inc.: Wallingford, CT, 2016.
(77) Case, D. A.; Darden, T. A.; Cheatham, T. E., III; Simmerling, C. L.; Wang, J.; Duke, R. E.; Luo, R.; Walker, R. C.; Zhang, W.; Merz, K. M.; et al. *AMBER 18*; University of California, San Francisco, 2018.
(78) Mukherjee, G.; Patra, N.; Barua, P.; Jayaram, B. A Fast Empirical GAFF Compatible Partial Atomic Charge Assignment Scheme for Modeling Interactions of Small Molecules with Biomolecular Targets. *J. Comput. Chem.* **2011**, *32*, 893−907.

https://dx.doi.org/10.1021/acs.jpcc.0c06539
J. Phys. Chem. C 2020, 124, 22383−22391

(79) Wang, J.; Wolf, R. M.; Caldwell, J. W.; Kollman, P. A.; Case, D. A. Development and Testing of a General Amber Force Field. *J. Comput. Chem.* **2004**, *25*, 1157−1174.
(80) Tretiak, S.; Chernyak, V.; Mukamel, S. Collective Electronic Oscillators for Nonlinear Optical Response of Conjugated Molecules. *Chem. Phys. Lett.* **1996**, *259*, 55−61.
(81) Wu, C.; Malinin, S. V.; Tretiak, S.; Chernyak, V. Y. Multiscale Modeling of Electronic Excitations in Branched Conjugated Molecules Using an Exciton Scattering Approach. *Phys. Rev. Lett.* **2008**, *100*, 057405−057405−4.
(82) Alfonso Hernandez, L.; Nelson, T.; Gelin, M. F.; Lupton, J. M.; Tretiak, S.; Fernandez-Alberti, S. Interference of Interchromophoric Energy-Transfer Pathways in π-Conjugated Macrocycles. *J. Phys. Chem. Lett.* **2016**, *7*, 4936−4944.

https://dx.doi.org/10.1021/acs.jpcc.0c06539
J. Phys. Chem. C 2020, 124, 22383−22391